JOURNAL OF THERMOPHYSICS AND HEAT TRANSFER
Vol. 10, No. 3, July–September 1996

Laminar Forced Convection at Zero Gravity to Water near the Critical Region

S. H. Lee* and John R. Howell†
University of Texas at Austin, Austin, Texas 78712

Numerical modeling is carried out to analyze the heat transfer and fluid flow for water in the critical region in laminar tube flow under zero-gravity conditions. The model considers variable density, specific heat, viscosity, and conductivity. The effect of proximity to the critical point is also considered. To accurately predict property distributions, the numerical grid is clustered in the region where property variation is severe. The results of the modeling provide heat transfer and flow characteristics including profiles of temperature and velocity, the heat transfer coefficient, and the friction factor in the developing region of the tube. Constant wall temperature and constant wall heat flux are considered, and pressure, inlet fluid temperature, and Reynolds number are used as parameters. The calculation results show differences compared from results based on constant properties, and provide insight into the effects of the large property variations on heat transfer.

Nomenclature

A = area, m^2
C_p = specific heat at constant pressure, kJ/kg °C
D = tube diameter, m
f = friction factor
h = heat transfer coefficient, W/m^2 °C
I = mapping property
i = enthalpy, J/kg
J = Jacobian of coordinate transformation
k = thermal conductivity, W/m °C
L = tube length, m
P = pressure, N/m^2
P_R = reduced pressure, P/P_c
Pr = Prandtl number
Q = heat flux, W/m^2
q_1, q_2, q_3 = geometric relations between coordinate systems
R = radius, m
Re = Reynolds number at inlet
r = radial distance, m
S = source term in conservation Eq. (9)
S^* = source term in conservation Eq. (10)
T = temperature, °C
T_{pc} = pseudocritical temperature, °C
U = velocity component along ξ direction
u = local velocity in axial direction, m/s
V = velocity component along η direction
v = local velocity in radial direction, m/s
z = axial distance, m
β = coefficient of thermal expansion, 1/°C
Γ = diffusion coefficient
η = transformed coordinate
μ = absolute viscosity, kg/s m
ξ = transformed coordinate
ρ = density, kg/m^3
τ = shear stress, N/m^2
Φ = viscous dissipation, J/kg m^2
ϕ = function variable

Subscripts
b = bulk condition
c = critical point value
in = inlet condition
w = wall condition

Superscript
i = iteration

Received Oct. 2, 1995; revision received Jan. 31, 1996; accepted for publication Feb. 1, 1996.

*Graduate Student, Department of Mechanical Engineering.
†Baker-Hughes Professor, Department of Mechanical Engineering. Fellow AIAA.

Introduction

OVER the past years, there has been rapid growth of research activities in supercritical heat transfer. Convection heat transfer to supercritical and near critical fluids is of great interest because of many applications, including the design of heat exchange equipment that uses water in powerplants, hydrogen in rockets, helium as a coolant in superconducting systems, and carbon dioxide in supercritical extraction systems. Although a significant amount of research has been carried out in this area, it is still difficult to predict accurately the heat transfer from fluids to surfaces at conditions near the pseudocritical temperature at supercritical pressure.

Near the critical point of water (T_c = 373.98°C and P_c = 22.06 MPa), there are large variations in the thermophysical and thermodynamic properties such as density, specific heat, viscosity, and conductivity (Figs. 1 and 2). In this region properties transition from liquid-like to gas-like behavior across the pseudocritical point as the temperature increases. Therefore, the governing equations for the fluid mechanics and heat transfer (Navier–Stokes and energy equations) cannot be uncoupled as in the constant property case. The extremely temperature-dependent properties near the pseudocritical point, particularly the density and isothermal compressibility, strongly affect the velocity profiles of the flow, and these velocity profiles in turn affect the heat transfer and the temperature distributions.

Because of the need for design of systems such as heat exchangers for operation near the critical region, there have been a considerable number of experimental[1–4] and theoretical[5–7] investigations of flow and heat transfer. Most of these studies are for turbulent flow, which is typical of most applications. These studies are to understand the observed phenomenon of degraded heat transfer in the tube near the pseudocritical temperature of the fluid for high wall heat flux, which results in hot spots on the tube wall. Most of the theoretical studies for turbulent flow have not accurately described the effect of prop-

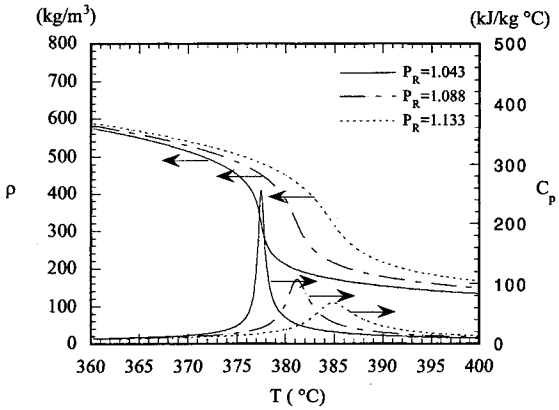

Fig. 1 Density and specific heat variation for water.

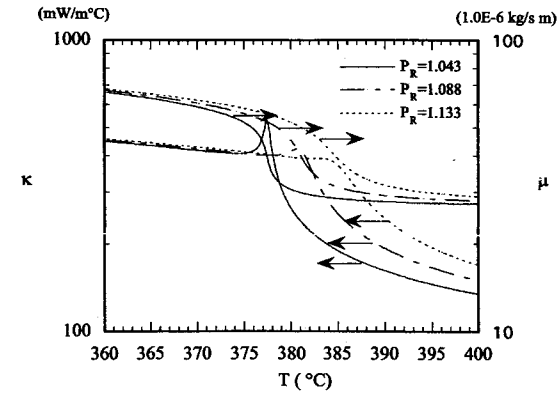

Fig. 2 Viscosity and thermal conductivity variation for water.

erty variations on modeling the turbulent Prandtl number, eddy diffusivity, and several other constants related with turbulence modeling. Most have used the general formulations without modification.

For low velocity (laminar) flow in a tube near the critical region, less research has been done. A few studies[8–11] have investigated numerically the problem of laminar flow in a vertical tube with or without buoyancy force for supercritical fluids such as CO_2, water, and helium, using the boundary-layer approximations. Koppel and Smith[10] modeled the case of constant heat flux, neglecting the radial velocity component and using implicit finite difference equations. Their results indicated some differences between near-critical and constant property results for the heat transfer coefficient, especially in the developing region near the pseudocritical point. Shenoy et al.[11] obtained numerical solutions without taking account of buoyancy forces for the case of constant wall temperatures, and demonstrated an increase in the heat transfer coefficient for the hydrodynamic entry region of tube flow near the critical region compared with the constant property solution. Dashevsky et al.[8] showed that there is a maximum value of heat transfer coefficient for developing flow in a tube, and that the maximum occurs when the fluid temperature in the tube is a little lower than the pseudocritical temperature. And the results showed that this peak value of heat transfer coefficient increases with a decrease of mass velocity and with an increase of heat flux. Bogachev et al.,[12] Vlakhov et al.,[13] and Valyuzhinich et al.[14] investigated supercritical fluids experimentally and suggested correlations for heat transfer coefficients in the laminar/transitional flow region. Their results show that there is a peak value in heat transfer coefficient in the developing region. And far from the critical region, the heat transfer characteristics are similar to those for the constant property case. Dashevsky et al.[9] inferred free convection effects from experimental data and suggested a heat transfer correlation for downflow of a supercritical fluid. Numerical and experimental results for laminar tube flow show that there are severe variable property effects on fluid flow and heat transfer and they cannot be neglected near the critical region.

Despite the several studies of tube flow for a near-critical fluid, the experimental data are sparse and the characteristics of heat transfer and fluid flow in a tube are not well understood. Because of the large number of variables and the difficult range of pressure and temperature, it is very tedious to get experimental measurements. The purpose of the present study is to understand the basic mechanisms and interactions of fluid flow and heat transfer and to predict laminar forced convection heat transfer to supercritical water in a tube. Unlike turbulent flow, there is no need to assume or model the turbulent Prandtl number and eddy diffusivity, and the results can predict well the effect of property variation near the critical region.

Numerical Modeling

The problem to be analyzed is heat transfer to near-critical water flowing through a smooth-walled circular tube. Flow enters a tube with a uniform velocity and constant temperature. The thermal conductivity of the tube wall is assumed so high that the thermal resistance through and along the wall can be neglected, and this additional parameter can be neglected.

The flow is assumed to be steady state and axisymmetric, and local thermodynamic equilibrium is assumed. Following are the governing continuity equation, Navier–Stokes equation, and energy equation in axisymmetric coordinates, which are used here.

Continuity:

$$\frac{1}{r}\frac{\partial}{\partial r}(\rho r v) + \frac{\partial}{\partial z}(\rho u) = 0 \tag{1}$$

Momentum equation:

$$\rho v\frac{\partial v}{\partial r} + \rho u\frac{\partial v}{\partial z} = -\frac{\partial p}{\partial r} + \frac{1}{r}\frac{\partial}{\partial r}(r\tau_{rr}) - \frac{\tau_{\theta\theta}}{r} + \frac{\partial}{\partial z}(\tau_{rz}) \tag{2}$$

$$\rho v\frac{\partial u}{\partial r} + \rho u\frac{\partial u}{\partial z} = -\frac{\partial p}{\partial z} + \frac{1}{r}\frac{\partial}{\partial r}(r\tau_{rz}) + \frac{\partial}{\partial z}(\tau_{zz}) \tag{3}$$

where

$$\tau_{rr} = \mu\left[2\frac{\partial v}{\partial r} - \frac{2}{3}(\nabla\cdot V)\right]$$

$$\tau_{\theta\theta} = \mu\left[2\frac{v}{r} - \frac{2}{3}(\nabla\cdot V)\right]$$

$$\tau_{zz} = \mu\left[2\frac{\partial v}{\partial z} - \frac{2}{3}(\nabla\cdot V)\right]$$

$$\tau_{rz} = \mu\left(\frac{\partial u}{\partial r} + \frac{\partial v}{\partial z}\right)$$

Energy equation:

$$\rho C_p(DT/Dt) = \mathrm{div}(k\nabla T) + \beta T(Dp/Dt) + \mu\Phi \tag{4}$$

The associated boundary conditions are

$$-z = 0 \text{ (inlet)} \qquad u = u_{in},\ v = 0,\ T = T_{in},\ P = P_{in}$$

$$-0 < z < L \quad \text{at } r = 0\text{: } \frac{\partial u}{\partial r} = 0,\ \frac{\partial v}{\partial r} = 0,\ \frac{\partial T}{\partial r} = 0$$

$$\text{at } r = R\text{: } u = 0,\ v = 0,\ T = T_w \text{ or } Q_w = -k\frac{\partial T}{\partial r}$$

The outlet is placed 30 diameters downstream of the tube inlet, and a linear extrapolation boundary condition is used. Thermodynamic and transport properties can be expressed as follows using the assumption of thermodynamic equilibrium condition:

$$\rho = \rho(T, p) \tag{5a}$$

$$C_p = C_p(T, p) \tag{5b}$$

$$\mu = \mu(T, p) \tag{5c}$$

$$k = k(T, p) \tag{5d}$$

For the properties of water, the code of Lester et al.[15] is used.

To get an accurate prediction of property distributions near the pseudocritical temperature in the tube, an adaptive grid method is used. This forces denser grids in the region where large variations of properties exist. In this grid generation, the variational approach of Brackbill and Saltzman[16] is used. The integral that measures the weighted volume variation over each mesh is

$$I = \int wJ \, dv, \qquad w = \left| \frac{1}{\rho} (\nabla \cdot \rho) \right|^2 \tag{6}$$

In this modeling, density is used as the variable for the weighting function because it has a rather smooth variation and represents the pseudocritical point very well compared with C_p near the critical region. To minimize the total integral value over the whole domain, the following extremum principle (Euler variation equation) is used:

$$\left(\frac{\partial}{\partial z} - \frac{\partial}{\partial \xi} \frac{\partial}{\partial z_\xi} - \frac{\partial}{\partial \eta} \frac{\partial}{\partial z_\eta} \right) (I) = 0 \tag{7a}$$

$$\left(\frac{\partial}{\partial r} - \frac{\partial}{\partial \xi} \frac{\partial}{\partial r_\xi} - \frac{\partial}{\partial \eta} \frac{\partial}{\partial r_\eta} \right) (I) = 0 \tag{7b}$$

The results with coefficients of the highest derivatives are expressed as follows:

$$b_1 z_{\xi\xi} + b_2 z_{\xi\eta} + b_3 z_{\eta\eta} + a_1 r_{\xi\xi} + a_2 r_{\xi\eta} + a_3 r_{\eta\eta} = C_1 \tag{8a}$$

$$a_1 z_{\xi\xi} + a_2 z_{\xi\eta} + a_3 z_{\eta\eta} + c_1 r_{\xi\xi} + c_2 r_{\xi\eta} + c_3 r_{\eta\eta} = C_2 \tag{8b}$$

The residuals of these highest derivative equations are used to check the convergence of grid generation. If an adaptive grid is used, the grid system is not necessarily orthogonal. Hence, the governing equations must be solved in generalized coordinates:

$$z = z(\xi, \eta)$$

$$r = r(\xi, \eta)$$

The governing conservation relations can be written in axisymmetric coordinates for the dependent variable ϕ in the following form:

$$\frac{\partial}{\partial z} (\rho u \phi) + \frac{1}{r} \frac{\partial}{\partial r} (r \rho v \phi) = \frac{1}{r} \frac{\partial}{\partial r} \left(r \Gamma \frac{\partial \phi}{\partial r} \right) + \frac{\partial}{\partial z} \left(\Gamma \frac{\partial \phi}{\partial z} \right) + S(r, z) \tag{9}$$

where $S(r, z)$ is the source term. With transformation to generalized coordinates, the general conservation equation becomes[17-19]:

$$\frac{\partial \rho U \phi}{\partial \xi} + \frac{\partial \rho V \phi}{\partial \eta} = \frac{\partial}{\partial \xi} \left[\frac{\Gamma}{J} \left(q_1 \frac{\partial \phi}{\partial \xi} - q_2 \frac{\partial \phi}{\partial \eta} \right) \right] + \frac{\partial}{\partial \eta} \left[\frac{\Gamma}{J} \left(-q_2 \frac{\partial \phi}{\partial \xi} + q_3 \frac{\partial \phi}{\partial \eta} \right) \right] + JS^*(\xi, \eta) \tag{10}$$

where $S^*(\xi, \eta)$ is the source term in ξ, η coordinates and

$$U = u(rr_\eta) - v(rz_\eta)$$

$$V = v(rz_\xi) - u(rr_\xi)$$

$$q_1 = (rz_\eta)^2 + (rr_\eta)^2$$

$$q_2 = (rz_\xi)(rz_\eta) + (rr_\xi)(rr_\eta)$$

$$q_3 = (rz_\xi)^2 + (rr_\xi)^2$$

$$J = (rz_\xi r_\eta) - (rz_\eta r_\xi)$$

The SIMPLE (Ref. 20) solution procedure developed for Cartesian coordinates can be extended to the above generalized (curvilinear) coordinates if the second and third terms on the right-hand side of Eq. (10) are included with the source term as in Shyy et al.[18] The equations of momentum, energy, and continuity (pressure correction) are solved iteratively with the renewal of water properties based on the pressure and temperature field. Relaxation factors are used for stability with values of 0.75 for velocities u and v, and 0.5 for temperature, and a staggered grid system is used. In this grid system each scalar variable such as temperature, pressure, and properties are defined at the grid centers. Velocity components are defined at the surfaces of the grid; u and U are at the midpoint of east and west surfaces, and v and V at the midpoints of north and south surfaces.

The convergence is checked with grid generation as well as by solving the governing equations of continuity, momentum, and energy. When the velocities and temperature satisfy the following convergence criteria for the grid system:

$$\left| \frac{\phi^{i+1} - \phi^i}{\phi^i} \right| < 10^{-3}, \quad \phi = u, v, \text{ and } T$$

a new grid system is generated. When the maximum grid position change is less than 10^{-2} compared with the former grid, the calculation is stopped. The total energy balance over the physical domain is also checked by comparing the total inlet and outlet enthalpy calculated from the respective radial distributions. Axial grids of 100, 200, and 300 points and radial grids of 15, 30, and 45 points were used to investigate the grid size effect on the calculation results. The difference between the results for heat transfer coefficient in the meshes of 200 × 30 and 300 × 45 for $z/D > 5$ is less than 1%. Hence, the grid of 200 × 30 was chosen for the calculations. The validity of the extrapolation boundary condition at the outlet of the tube was checked by comparison with the results for longer tubes. All calculations are carried out on an IBM RISC System/6000. To verify the program code, calculations were compared with other existing results for the variable property case[21] and constant property case[22] in tube flow. The predictions agreed very well with other results.

Results and Discussion

Near the critical region ($1 < P_R < 1.15$), there is steep variation in thermodynamic and thermophysical properties with temperature and pressure because of the characteristic phase transition between liquid and gas. With heat transfer, fluid

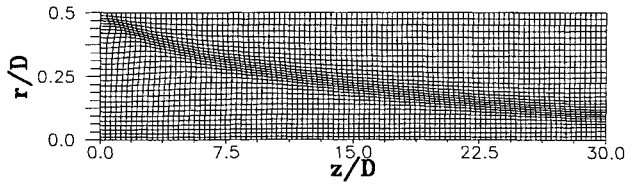

Fig. 3 Typical grid distribution by adaptive grid method.

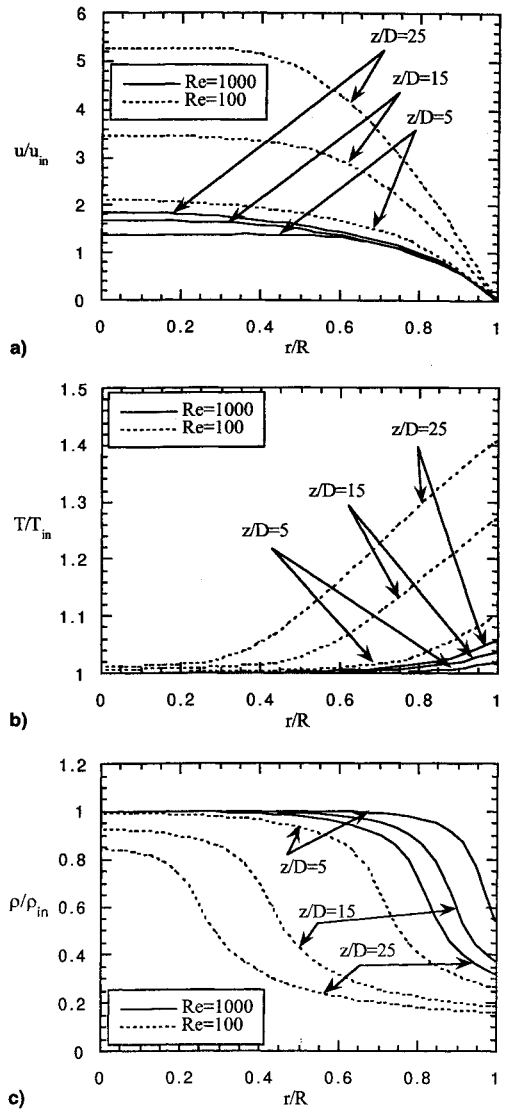

Fig. 4 Radial profiles of a) velocity, b) temperature, and c) density at several axial distances for $Re = 1 \times 10^2$ and $Re = 1 \times 10^3$; constant wall heat flux ($T_{in} = 375°C$, $P = 24$ MPa, $Q_w = 2$ kW/m^2).

passes through the pseudocritical point where there is the maximum property gradient with temperature for a specified pressure. As the property variation effects are strongly coupled with the flowfield, it is difficult to predict fluid flow and heat transfer characteristics and find which one has the major effect. In this analysis, variations of specific heat, thermal conductivity, density, and viscosity are considered, but body forces are not included, so that buoyancy terms are neglected in the momentum equation. This is to simplify the phenomena and understand the effect of property variation. The results are applicable to zero-gravity conditions; however buoyancy effects in nonzero gravity fields are important in laminar flow,[23] and in turbulent flow are apparently related to observed deterioration in heat transfer in a tube. In this analysis, constant wall heat flux and constant wall temperature boundary conditions are considered. Figure 3 shows a typical grid generation using the adaptive grid method. It can be seen that the grid is clustered in some regions and this occurs where there is large variation of properties. With this grid system, properties can be predicted well in the tube.

Figure 4a shows the entrance region velocity profiles at various downstream distances in a tube for Re of 1×10^2 and 1×10^3 for the same heat flux boundary conditions ($Q_w = 2$ kW/m^2). There is some difference between the two developing velocity profiles. At $Re = 1000$ the developing velocity appears similar to the case of laminar flow with constant properties. But it is seen that the velocity profile for $Re = 100$ has not approached the fully developed parabolic profile, which is typical of laminar flow when the properties are temperature independent. The distances z/D for laminar fully developed flow for constant properties are about 5 and 50 for the Reynolds numbers of 1×10^2 and 1×10^3. The velocity at the centerline increases rapidly with z for $Re = 1 \times 10^2$ compared with $Re = 1 \times 10^3$. This is related with the density change caused by the heat transfer from the wall. As the fluid temperature increases with heat transfer through the pseudocritical temperature, the fluid density decreases very rapidly. For $Re = 1 \times 10^2$, this effect reaches far from the wall inside the tube, and to satisfy mass conservation the velocity must increase along the tube.

Water temperature profiles in the tube are shown in Fig. 4b. In the temperature profiles, it seems that there is no anomalous behavior as observed in the velocity profiles. Note that the temperature gradient at the wall for $Re = 1 \times 10^2$ is a little steeper than for $Re = 1 \times 10^3$. In the constant property case the gradient should be the same along the tube for $Re = 1 \times 10^2$ and $Re = 1 \times 10^3$. This effect is related to the temperature dependent water conductivity along the wall. For $Re = 1 \times 10^2$ the wall temperature along the tube ($z/D > 5$) is higher than the pseudocritical temperature because of heat transfer, but for $Re = 1 \times 10^3$ wall temperature is mostly less than that temperature. Hence, the water conductivity near the wall for $Re = 1 \times 10^2$ is smaller than that for $Re = 1 \times 10^3$. With the same heat flux prescribed at the wall, a smaller conductivity results in a higher wall temperature gradient for the same wall heat flux. Also note that, near the pseudocritical temperature, where the specific heat is relatively high and has large variation, heat transfer is dominated by convection rather than diffusion.

Figure 4c shows the density profile in the developing region. It can be seen that at each downstream distance, there is large variation of density across the tube section and the pseudocritical temperature point moves radially toward the centerline. Compared with the large variation of density (and other properties) in the cross section of the tube, temperature variations are relatively small.

Figures 5a and 5b show the velocity and temperature profiles in the entrance region for inlet Reynolds numbers of 1×10^2 and 1×10^3 for the case of constant wall temperature of 400°C. The pseudocritical temperature at the given inlet pressure of 24 MPa is about 382°C. For the given inlet temperature of 375°C, large property variations across the tube radius are expected. The profiles have similar characteristics to the constant heat flux boundary condition. At $Re = 1 \times 10^2$, the velocity profile develops and the centerline velocity increases very rapidly because of the density decrease by heat transfer. But at $Re = 1 \times 10^3$, the velocity profile develops like the constant property case. For the temperature profiles, anomalous behavior as seen for the velocity profile cannot be found. The temperature gradient at the wall in the tube is larger for the case of high Reynolds number ($Re = 1 \times 10^3$), so that the heat flux from the wall is higher than for the low Reynolds number case ($Re = 1 \times 10^2$). Figure 5c shows the density profiles in the tube. It can be seen that the large density variation region moves faster toward the tube centerline for low Reynolds number. Although there is a decrease in density with

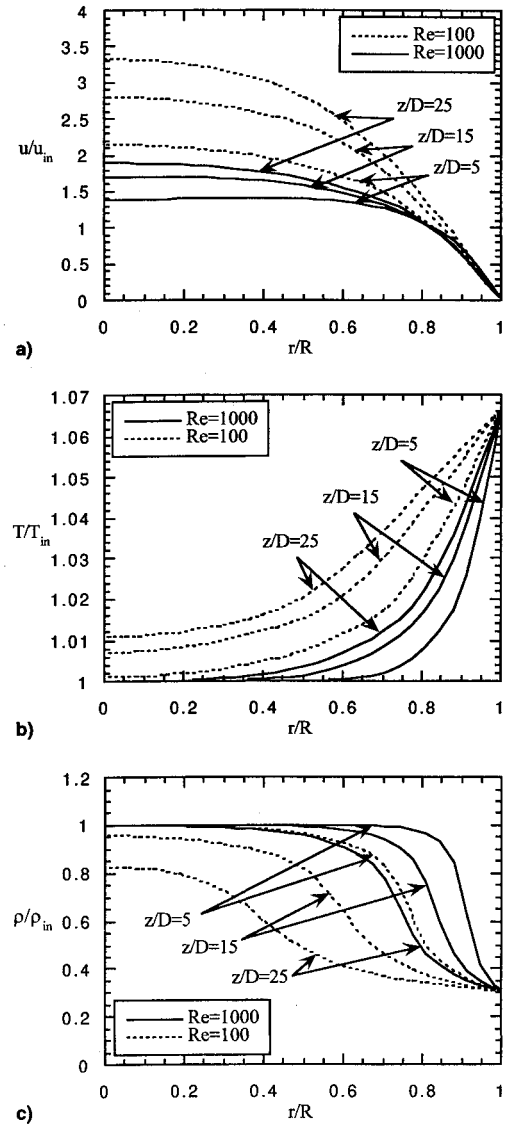

Fig. 5 Radial profiles of a) velocity, b) temperature, and c) density at several axial distances for $Re = 1 \times 10^2$ and $Re = 1 \times 10^3$; constant wall temperature ($T_{in} = 375°C$, $P = 24$ MPa, $T_w = 400°C$).

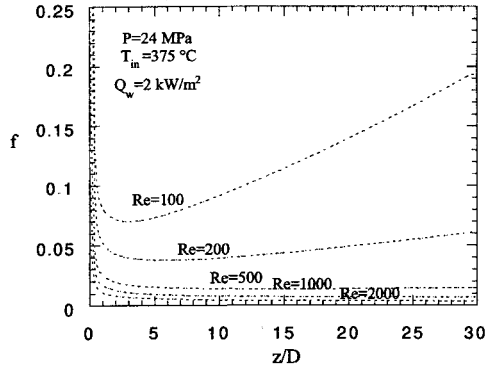

Fig. 6 Friction factor distributions along the tube in the constant wall heat flux case.

heat transfer, the momentum flux increases along the tube because of the increase of velocity which results from the mass conservation.

The friction factor is

$$f = 8\tau_w/(\rho_{in}u_{in}^2) \tag{11}$$

and its distribution is shown for various Reynolds numbers in Fig. 6. For low Reynolds numbers ($Re = 1 \times 10^2$ and $Re = 2 \times 10^2$), the friction factor first decreases near the entrance and then, after some distance, increases along the tube. This increase occurs because of the local momentum increase. Viscosity at the wall decreases due to heat transfer, but the increase in velocity gradient at the wall causes a net increase in the friction factor. This increase continues until there is little variation of properties, especially density, across the tube section. For high Reynolds numbers ($Re > 5 \times 10^2$), this effect is rather small.

Figure 7 shows the heat transfer coefficients for various Reynolds numbers. As mass flow rate increases, heat transfer coefficient increases even if there is large variation of properties inside the tube. The results show some differences compared with the constant property solution and the differences depend on Reynolds number. Far from the entrance region, where flow is fully developed and there is little variation of properties, the heat transfer coefficient should be independent of Reynolds number in laminar flow. In the heat transfer coefficient calculation, the bulk fluid temperature is defined as follows:

$$T_b = \int_A \rho u C_p T \, dA \Big/ \int_A \rho u C_p \, dA \tag{12}$$

Equation (12) includes the effect of variation of properties in the use of density and specific heat. Figure 8 shows the heat transfer coefficient for various inlet temperatures. It can be seen that heat transfer coefficient characteristics depend on whether the inlet water temperature is below the pseudocritical temperature. When the inlet water temperature is lower than the pseudocritical temperature such as $T_{in} = 350$ and 325°C,

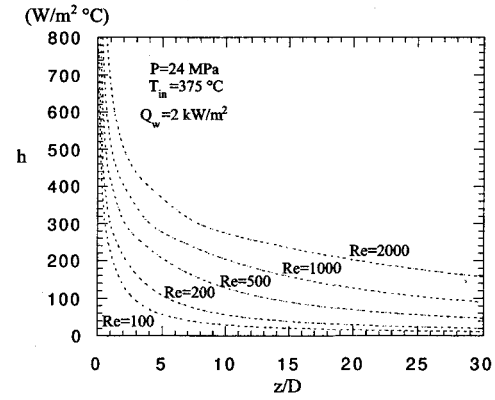

Fig. 7 Heat transfer coefficient distributions along the tube for various Reynolds numbers in the constant wall heat flux case.

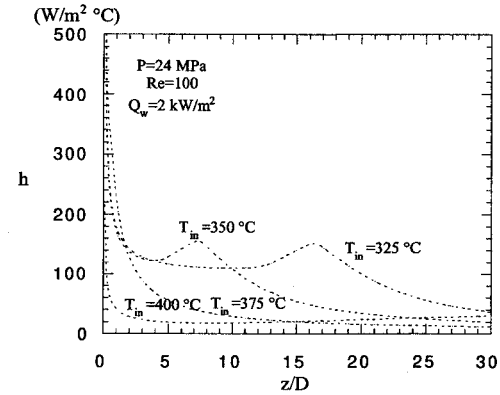

Fig. 8 Heat transfer coefficient distributions along the tube for various inlet water temperatures in the constant wall heat flux case.

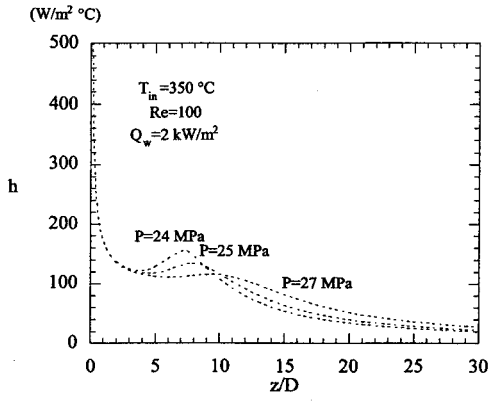

Fig. 9 Heat transfer coefficient distributions along the tube for various pressures in the constant wall heat flux case.

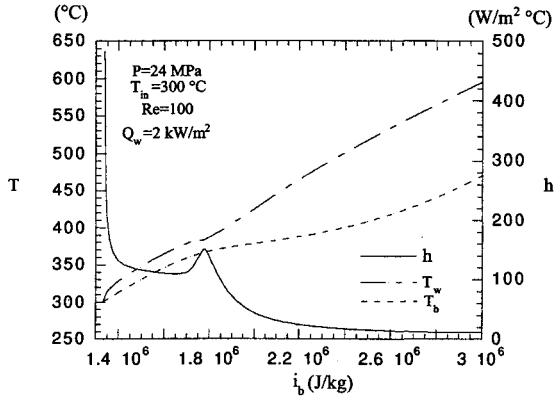

Fig. 10 Bulk and wall temperature and heat transfer coefficient distributions along the tube.

there is a peak in heat transfer coefficient distribution along the tube. This happens when the bulk temperature of water is close to the pseudocritical temperature. The peak in heat transfer coefficient is because of the high specific heat value near the pseudocritical temperature. High heat capacity increases heat transfer by the convection mechanism. The heat transfer coefficient decreases after the peak. Before T_b reaches T_{pc}, the fluid has the characteristics of a liquid, and after T_b passes T_{pc} it has gas-like characteristics. Hence, the heat transfer coefficient is higher so long as T_b remains lower than T_{pc} after an initial developing distance ($z/D > 5$). If the inlet water temperature is higher than the pseudocritical temperature, there is no severe variation of properties with temperature and the heat transfer coefficient distribution is similar to the constant property case.

Figure 9 shows the heat transfer coefficient for various inlet pressures. The peak in heat transfer coefficient increases as the pressure approaches to the critical pressure, again because of the increase of maximum specific heat with pressure at the pseudocritical point. The pseudocritical temperature depends on the pressure, and as the pressure in the tube increases, the pseudocritical temperature increases, and the axial position of the peak is moved downstream.

Figure 10 shows the wall and bulk temperatures and the heat transfer coefficient along the tube for a long tube ($L = 100D$). Near the peak of the heat transfer coefficient, the bulk temperature of water is lower than the pseudocritical temperature and the wall temperature is a little higher. The rate of wall temperature does not change much after the peak, but the bulk temperature increases slowly near the pseudocritical temperature along the tube. This is again because of the transition from the liquid-like phase to the gas-like phase of water with the corresponding change of properties. Hence, the temperature difference between the wall and the bulk increases and the heat transfer coefficient decreases, even though there is acceleration of water along the tube.

Conclusions

Numerical modeling is performed for laminar forced convection heat transfer in a tube near the critical region of water, accounting for all property variations such as density, specific heat, viscosity, and conductivity. Using the results of numerical modeling in this study, the following conclusions can be drawn:

At low Reynolds number ($\approx 1 \times 10^2$), when there is a pseudocritical temperature region inside the tube, there is acceleration of the water along the tube, and the centerline velocity increases very rapidly compared with the fully developed velocity profile in laminar flow. However, temperature profiles show little anomalous behavior despite large property variations across the tube section.

The friction factor increases after some point in the developing region because of the momentum increase caused by the density decrease with heat transfer. Heat transfer coefficients depend on many parameters such as pressure, inlet water temperature, and Reynolds number. When the bulk temperature approaches the pseudocritical temperature, the heat transfer coefficient has a peak value. And as the pressure approaches the critical pressure, the peak in heat transfer coefficient increases.

References

[1]Kurganov, V. A., and Kaptilnyi, A. G., "Flow Structure and Turbulent Transport of a Supercritical Pressure Fluid in a Vertical Heated Tube Under the Conditions of Mixed Convection. Experimental Data," *International Journal of Heat and Mass Transfer*, Vol. 36, No. 13, 1993, pp. 3383–3392.

[2]Shitsmann, M. E., "Impairment of the Heat Transmission at Supercritical Pressure," *Teplofizika Vysokikh Temperatur*, Vol. 1, No. 2, 1963, pp. 237–243.

[3]Watts, M. J., and Chou, C. T., "Mixed Convection Heat Transfer to Supercritical Pressure Water," *Proceedings of the International Heat Transfer Conference*, Vol. 3, Hemisphere, New York, 1982, pp. 495–500.

[4]Yamagata, K., Nishikawa, K., Hasegawa, S., Fujii, T., and Yoshida, S., "Forced Convective Heat Transfer to Supercritical Water Flowing in Tubes," *International Journal of Heat and Mass Transfer*, Vol. 15, No. 12, 1972, pp. 2575–2593.

[5]Hauptmann, E. G., and Malhotra, A., "Axial Development of Unusual Velocity Profiles Due to Heat Transfer in Variable Density Fluids," *Journal of Heat Transfer*, Vol. 102, No. 1, 1980, pp. 71–74.

[6]Koshizuka, S., Takano, N., and Oka, Y., "Numerical Analysis of Deterioration Phenomena in Heat Transfer to Supercritical Water," *International Journal of Heat and Mass Transfer*, Vol. 38, No. 16, 1995, pp. 3077–3084.

[7]Polyakov, A. F., "Heat Transfer Under Supercritical Pressures," *Advances in Heat Transfer*, edited by James P. Hartnett and Thomas F. Irvine Jr., Vol. 21, Academic, New York, 1991, pp. 1–53.

[8]Dashevsky, Y. M., and Malkovsky, V. I., "Heat Exchange with Laminar Upflow of Supercritical Helium in a Gravitational Field," *Cryogenics*, Vol. 25, Nov. 1985, pp. 658, 659.

[9]Dashevsky, Y. M., Malkovsky, V. I., Miropolsky, Z. L., Sakovich, N. D., and Khasanov-agayev, L. R., "Effect of Thermogravitation on Heat Transfer in Up or Down Pipe Flow of Supercritical Fluids," *Heat Transfer—Soviet Research*, Vol. 18, No. 6, 1986, pp. 109–114.

[10]Koppel, L. B., and Smith, J. M., "Laminar Flow Heat Transfer for Variable Physical Properties," *Journal of Heat Transfer*, Vol. 84, No. 2, 1962, pp. 157–163.

[11]Shenoy, S. U., Jagadish, B. S., and Sharma, G. K., *Proceedings of the National Heat Mass Transfer Conference* (Bombay, India), Paper HMT-C19-85, 1975.

[12]Bogachev, V. A., Yeroshenko, V. M., and Yaskin, L. A., "Heat Transfer Associated with an Ascending Flow of Supercritical Helium in a Heated Tube with $Re < 2300$ at the Entry," *Teplofizika Vysokikh Temperatur*, Vol. 21, No. 1, 1983, pp. 101–106.

[13]Vlakhov, E. S., Miropol'skii, Z. L., and Khasanov-agaev, L. R., "Heat Transfer to a Supercritical Medium with Mixed Convection and Rising Flow in Heated Tubes," *Teploenergetika*, Vol. 28, No. 11, 1981, pp. 69–71.

[14]Valyuzhinich, M. A., Eroshenko, V. M., and Kuznetsov, E. V., "Heat Transfer to Fluids at Supercritical Pressure in the Entrance Region Under Conditions of Strong Nonisothermicity," *Teploenergetika*, Vol. 32, No. 1, 1985, pp. 64–66.

[15]Lester, H., John, S. G., and George, S. K., *Steam Tables*, Hemisphere, New York, 1984.

[16]Brackbill, J. U., and Saltzman, J. S., "Adaptive Zoning for Singular Problems in Two Dimensions," *Journal of Computational Physics*, Vol. 46, No. 3, 1982, pp. 342–368.

[17]Braaten, M., and Shyy, W., "A Study of Recirculating Flow Computation Using Body-Fitted Coordinates: Consistency Aspects and Mesh Skewness," *Numerical Heat Transfer*, Vol. 9, No. 5, 1986, pp. 559–574.

[18]Shyy, W., Tong, S. S., and Correa, S. M., "Numerical Recirculating Flow Calculation Using a Body-Fitted Coordinate System," *Numerical Heat Transfer*, Vol. 8, No. 1, 1985, pp. 99–113.

[19]Thompson, J. F., Warsi, Z. U. A., and Mastin, C. W., *Numerical Grid Generation*, Elsevier, New York, 1985.

[20]Patankar, S. V., *Numerical Heat Transfer and Fluid Flow*, Hemisphere, Washington, DC, 1980.

[21]Worsøe-Schmidt, P. M., and Leppert, G., "Heat Transfer and Friction for Laminar Flow of Gas in a Circular Tube at High Heating Rate," *International Journal of Heat and Mass Transfer*, Vol. 8, No. 10, 1965, pp. 1281–1301.

[22]Zeldin, B., and Schmidt, F. W., "Developing Flow with Combined Forced-Free Convection in an Isothermal Vertical Tube," *Journal of Heat Transfer*, Vol. 94, No. 2, 1972, pp. 211–223.

[23]Lee, S. H., and Howell, J. R., "Gravitational Effects on Laminar Forced Convection Heat Transfer in a Vertical Tube for CO_2 Near the Critical Region," *Symposium on Thermal Science and Engineering in Honor of Chancellor Chang-Lin Tien*, Univ. of California at Berkeley, CA, Nov. 1995, pp. 11–17.